AIP | Review of Scientific Instruments

Optomechanical design and construction of a vacuum-compatible optical parametric oscillator for generation of squeezed light

A. R. Wade, G. L. Mansell, T. G. McRae, S. S. Y. Chua, M. J. Yap, R. L. Ward, B. J. J. Slagmolen, D. A. Shaddock, and D. E. McClelland

Citation: Review of Scientific Instruments **87**, 063104 (2016); doi: 10.1063/1.4953326
View online: http://dx.doi.org/10.1063/1.4953326
View Table of Contents: http://scitation.aip.org/content/aip/journal/rsi/87/6?ver=pdfcov
Published by the AIP Publishing

Optomechanical design and construction of a vacuum-compatible optical parametric oscillator for generation of squeezed light

A. R. Wade,[1] G. L. Mansell,[1] T. G. McRae,[1,a)] S. S. Y. Chua,[2] M. J. Yap,[1] R. L. Ward,[1] B. J. J. Slagmolen,[1] D. A. Shaddock,[1] and D. E. McClelland[1]
[1]*Centre for Gravitational Physics, Department of Quantum Science, Research School of Physics and Engineering, The Australian National University, Canberra, ACT 2601, Australia*
[2]*Laboratorie Kastler Brosssel, UPMC-Sorbonne Universites, CNRS, ENS-PSL Research University, College de France, Paris, France*

(Received 4 February 2016; accepted 23 May 2016; published online 10 June 2016)

With the recent detection of gravitational waves, non-classical light sources are likely to become an essential element of future detectors engaged in gravitational wave astronomy and cosmology. Operating a squeezed light source under high vacuum has the advantages of reducing optical losses and phase noise compared to techniques where the squeezed light is introduced from outside the vacuum. This will ultimately provide enhanced sensitivity for modern interferometric gravitational wave detectors that will soon become limited by quantum noise across much of the detection bandwidth. Here we describe the optomechanical design choices and construction techniques of a near monolithic glass optical parametric oscillator that has been operated under a vacuum of 10^{-6} mbar. The optical parametric oscillator described here has been shown to produce 8.6 dB of quadrature squeezed light in the audio frequency band down to 10 Hz. This performance has been maintained for periods of around an hour and the system has been under vacuum continuously for several months without a degradation of this performance. *Published by AIP Publishing.* [http://dx.doi.org/10.1063/1.4953326]

I. INTRODUCTION

Improving the sensitivity of gravitational wave (GW) detectors[1–4] will require reliable and stable vacuum squeezed light sources that are able to operate under high vacuum. Squeezed light injection, from outside the interferometer vacuum, has already been demonstrated at the laser interferometer observatory GEO 600 GW detector[1,5] and the (LIGO) Hanford detector.[6] An improvement in the respective shot noise of 2.15 dB and 3.7 dB[7] for these detectors was observed. Losses of 56% (LIGO H1) and 38% (GEO 600) were consistent with optical losses and phase noise. Squeezed light is now in routine use in the GEO 600 detector.

While previous work has described single pass nonlinear sources operating under high vacuum,[8–10] this work describes the techniques necessary to build a doubly resonant travelling wave optical parametric oscillator (OPO) with a near monolithic glass construction. The bow-tie OPO design has a large degree of optical isolation (40 dB)[11] and has produced the highest levels of squeezing at acoustic frequencies.[12] With this system, a reduction in the quantum noise of 8.6 dB down to 10 Hz under high vacuum was observed.[13] This performance is comparable to nonlinear devices operated under ambient laboratory conditions.[6,11,14,15]

The OPO resonator presented here is constructed from fused silica as it is expected to offer superior length stability and long term alignment stability. This stability is critical to the reduction of squeezing level fluctuations and also the phase noise (or squeezing angle jitter) that results from the unstable rotation of the squeezing ellipse of the squeezed states investigated in this work.[16] However the design and construction techniques for this type of resonator are not straight forward and will therefore be the focus of this article. For information regarding the performance and integration of this OPO as a source of squeezed light, we refer the interested reader to Wade *et al.*[13] and references therein.

II. OPO RESONATOR DESIGN

A squeezed vacuum field has a smaller variance in the squeezed quadrature and a larger variance in the orthogonal, anti-squeezed, quadrature than a vacuum field. The average level of measured squeezing is therefore degraded when squeezing angle jitter occurs faster than the measurement time, whereas the long term stability of the measurement is limited when the jitter is slower than the measurement time. This stability is especially important in GW interferometers and future GW astronomy, where the measurement frequencies may be as low as 10 Hz and long term stability over several months is required. A monolithic glass structure is estimated to have a RMS (root mean squared) phase noise of only 0.1 mrad and squeezed quadrature fluctuations due to OPO length noise become negligible.[17]

This prototype design is based on the LIGO output mode cleaner (OMC).[18] The breadboard base for the resonator is made from fused silica with an expansion coefficient of 0.52 ppm/K[18] and a strain of approximately 1.794×10^{-7}. The mirror mounts are directly bonded to the breadboard using solution assisted optical contacting, rather than using glue. Glue can introduce minor changes in the degree of vertical alignment of the mirror mounts and optical contacting is reversible compared to silicate bonding. The mirror mounts

a)Electronic mail: Terry.Mcrae@anu.edu.au

have holes drilled for beam access from the back of the mirrors and dimensions for the mirror mounts are based on the OMC documentation for advanced LIGO,[18] which is optimised for minimising mechanical modes at the node point of the incident beam.

The chosen cavity configuration was a single ended bow-tie traveling wave cavity (Fig. 1) as it offers intrinsic optical isolation of 40 dB over the equivalent standing wave cavity[11] and therefore reduces the need for Faraday isolators. This is especially important for GW detection as backscattered light can create spurious signals that can potentially mask genuine gravitational wave signals.[19–21]

The principal choice of cavity coupling is selected by the coating on the input-output coupler at the two operating wavelengths (1064 nm and 532 nm). The reflectivity of this mirror at the fundamental and harmonic (pump) wavelengths was chosen to meet the design requirements such that the escape efficiency, the ratio of out-coupling to total losses is maximised and that the input pump power is resonantly enhanced to minimise the required input pump power. The cavity linewidths have been selected such that injected sidebands for the modified coherent lock[11,22] are ideally outside the cavity resonance at 1064 nm to avoid seeding at the main laser frequency but where the pump (532 nm) linewidth is broad enough to provide sufficient non-linear interaction strength for sampling the relative phase of the pump via the sidebands. These considerations were detailed in the previous bow-tie OPO designed to operate in standard laboratory conditions that were made with standard adjustable mirror mounts. We refer the interested reader to Stefszky[12] for a comprehensive treatment. A summary of the parameters of the OPO operated in vacuum is provided in Table I.

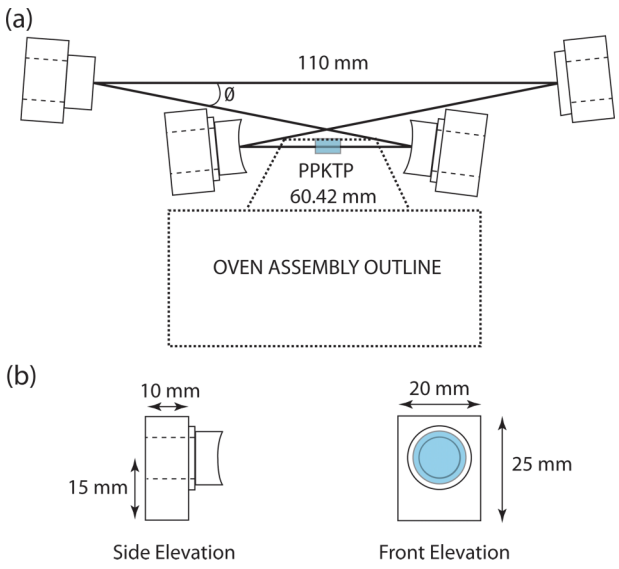

FIG. 1. (a) A scale drawing (top view) of the OPO resonator and optics, where $\phi/2 = 6°$ is the angle of incidence (AOI). The dotted line is an approximate outline of the position of the oven assembly and the [potassium titanyl phosphate (PPKTP)] crystal holder, see Fig. 5 for detail. The distance between the flat mirrors is 110 mm and the distance between the curved mirrors is 60.4 mm. (b) Side and front elevation of a glass mirror mount that is to be contact bonded to the breadboard.

A. Choice of cavity parameters

The degenerate OPO is a second-order ($\chi^{(2)}$) nonlinear process where the nonlinear element (Section II B) is a periodically poled potassium titanyl phosphate crystal (PPKTP). For maximum nonlinear gain, the optimal waist size was calculated from the Boyd-Kleinman method[23] and is approximately 30 μm at 1064 nm for our application with a 10 mm long PPKTP crystal.[12] This waist has to be achieved within a stable resonant mode of the OPO of a compact size. A 6° angle of incidence (AOI) to the curved mirrors has previously produced an acceptable level of mode astigmatism from the OPO resonator.[12] The resonator stability is designed using paraxial resonator theory where we use a generalised version of the two-mirror cavity g parameter. This parameter, m, is defined as $m = \mathrm{Tr}\mathbf{M}_{\mathrm{rt}}/2$, where $\mathrm{Tr}\mathbf{M}_{\mathrm{rt}}$ is the round trip ABCD matrix.[24]

Figure 2 outlines the initial procedure used to determine the radius of curvature (ROC) of the resonator mirrors. We first place upper and lower bounds on the stability with respect to the curved mirror separation and the radius of curvature (ROC). A −50 mm ROC was chosen to give the tightest possible focusing, limited by the physical dimensions of the cavity, while keeping the footprint of the cavity to a minimum. Figure 3 shows the primary (crystal) waist plotted as a function of the flat mirror separation as curved mirror separation is adjusted such that cavity stability is held at $m = 0$. The required waist of 30 μm is then achieved at a flat mirror separation of 110 mm where the ideal curved mirror separation is 60.4 mm for the sagittal plane at its most stable location ($m = 0$).

We minimise astigmatism in the primary (in crystal) waist at the expense of the secondary waist as astigmatism of the secondary waist may be corrected once coupled out of the cavity. The cavity waists and stability may be computed as a function of curved mirror separation for cavity parameters selected above. The cavity's tangential and sagittal waists are plotted in Fig. 4. Computed values for waist size at the midpoint between the peak stability of the two planes at the primary (crystal) waist are 30.2_{s} μm and 29.9_{t} μm in the sagittal and tangential planes, respectively. The secondary waist was found to be 205.4_{s} μm and 193.0_{t} μm at the midpoint. Waist sizes are therefore well matched in the primary (in crystal) waist with some astigmatism in the secondary waist. The squeezed beam coupled out of the cavity is therefore slightly astigmatic, having the same mode as the secondary waist at an identical distance beyond the input-output coupler. This waist mismatch may lead to mode mismatch to the modes and fields of measurement devices or apparatus it is coupled into and must be corrected for ideal mode matching.

B. The OPO crystal

The OPO cavity presented here is resonant on both the pump and fundamental frequencies. This allows perfect mode matching of the intracavity fields and allows the pump field to be easily used as a cavity length control signal. However this design requires precision thermal management (Section II C)

TABLE I. Cavity parameters for the semi-monolithic glass optical parametric oscillator operated in vacuum.

Cavity parameter	Symbol	Value
Fundamental wavelength	λ_f	1064 nm
Second harmonic (pump) wavelength	λ_p	532 nm
Cavity round trip length	L	345 mm
Free spectral range	FSR	849 MHz
Finesse (1064 nm)	F_{1064}	37
Finesse (532 nm)	F_{532}	17.6
Curved mirror ROC	ROC	−50 mm
Cavity linewidth fundamental	$\Delta\nu_{1064}$	23 MHz
Cavity linewidth pump	$\Delta\nu_{532}$	48 MHz
Waist size within crystal (1064 nm)	$w_{o(1064)}$	30 μm
Waist size within crystal (532 nm)	$w_{o(532)}$	21.2 μm
Out coupled beam sagittal waist at 1064 nm	$w_{out,s(1064)}$	205.4_s μm
Out coupled beam tangential waist at 1064 nm	$w_{out,t(1064)}$	193.0_t μm
In-out coupler reflectivity fundamental	$R_{in/out(1064)}$	0.845
In-out coupler reflectivity pump	$R_{in/out(532)}$	0.70
Total intra-cavity loss fundamental	T^l_{1064}	0.0037
Total intra-cavity loss pump	T^l_{532}	0.046
Escape efficiency	η_{esc}	97.9%

to minimise photothermal effects in the PPKTP crystal from the resonantly enhanced pump field and also for dispersion compensation. The PPKTP crystal is quasi-phase-matched and anti-reflection coated at both wavelengths (532 nm and 1064 nm) and has a 1.15° angle on the facet facing toward (or away) from the pump light. This angle compensates for dispersion and allows three translational positions of the crystal that satisfy the dual resonance condition.[12,25] A vacuum compatible motorised translation stage (Newport 8081M-UHV) is used to compensate for the shift in dispersion when moving from air to a vacuum environment. The poling is stopped about 1 mm before the angled facet to aid with the polishing. Poling is approximately 9 μm,[26] giving a phase matching temperature of 30–35 °C. PPKTP was chosen for its high nonlinear gain coefficient and low phase matching temperature.[27,28]

C. Temperature control

The mounting, translation, and temperature control of the nonlinear crystal are integral to the performance of the squeezer and affect both the non-linear conversion through phase matching control and the dispersive correction of the cavity's fundamental and harmonic fields. The operation of the double resonant bow-tie OPO under vacuum adds additional thermal management considerations, where radiation and conduction are the only mechanisms for heat transfer. Construction materials must be free of hydrocarbon contaminates and other materials that may outgas in vacuum.

The construction of the oven is illustrated in Fig. 5. The crystal is held between a copper cradle ("L"-piece) and rectangular block clamped from above with an M3 screw. The crystal clamping assembly was designed to hold the crystal with the largest possible contact area for thermal conduction and leave the outer edges unobstructed to avoid clipping the cavity fields. The crystal holding assembly was fixed from the sides with two M4 polyether ether ketone (PEEK) screws to a baseplate used as a heat sink. Sandwiched between these elements was a Peltier thermoelectric device (Laird Technologies, HOT20.31.F2A.0909) for active temperature

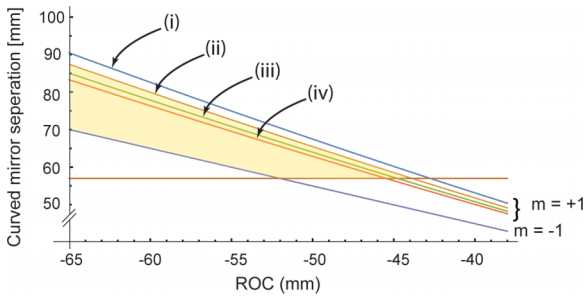

FIG. 2. The shaded region shows the range over which the cavity is stable, from m = 1 to m = −1, where the flat mirror separation is (i) 90 mm, (ii) 110 mm, (iii) 130 mm, and (iv) 150 mm. The horizontal line is the minimum curved mirror separation for stability (57 mm).

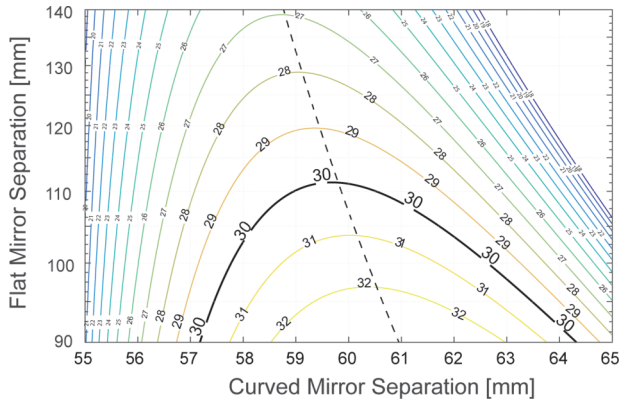

FIG. 3. The contour lines show the change of cavity waist (μm) with cavity dimension for a −50 mm ROC. The dashed line represents the maximum cavity stability. For a waist of 30 μm, the 110 nm flat mirror separation was chosen to align with this mirror ROC.

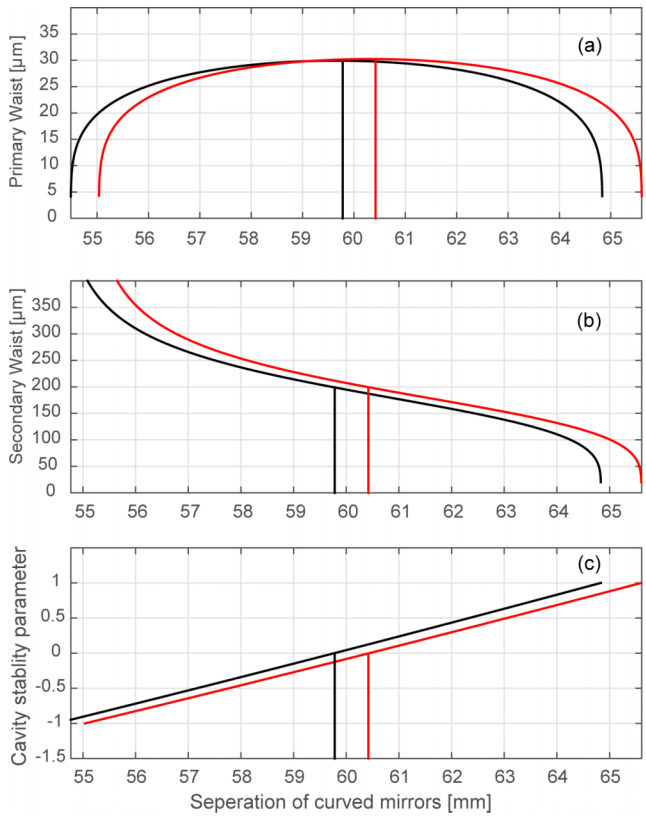

FIG. 4. The tangential (black lines) and sagittal (red lines) cavity waists and stability as a function of curved mirror (ROC = −50 mm) separation for the bow-tie resonator with a flat mirror separation of 110 mm. (a) The primary waist, (b) the secondary waist, and (c) the cavity mode stability parameter.

control of the crystal to within a fraction of a degree. For vacuum compatibility, the Peltier unit was not hermetically sealed with filling agents, as is the case of many such commercially available units. The semiconductor junctions were exposed, avoiding pockets of gas that might burst under vacuum and damage components. Either side of the Peltier and crystal elements is a thin (100 μm) layer of indium foil to improve thermal conduction in a vacuum environment. The temperature of the crystal holding assembly was measured with a miniature NTC thermistor (10k Siemens-Matsushita B57861 series) held into a tightly fitting hole in the back of the assembly with a tapped grub screw and packed with indium foil. The signal was fed back to a Newport 3040 Temperature Controller, which provided actuation current to the Peltier in a (PI) control loop.

In order to minimise the thermal load, the total mass of the crystal holder was kept to a minimum of 8.95 g, giving a heat capacity of 5.6 J/K. This minimises the reaction time and excess heat generated in pumping heat in and out of the oven mount with the Peltier that is slow to dissipate in a vacuum environment. The minimum dimensions were limited by the need to fit the thermistor into the back of the assembly and the necessary lengths to tap threads to hold the top M3 screw and grub screw fixing the thermistor in place. Under vacuum, the estimated radiated heat loss of the crystal holding assembly is given by the Stefan-Boltzmann Law,

$$P_{\text{net}} = \epsilon_{\text{Cu}} \sigma A (T^4 - T_{\text{env}}^4) \approx 2.9 \text{ mW}. \quad (1)$$

Here A is the total exposed surface area of 725 mm^2, $\epsilon_{\text{Cu}} = 0.05$ is the emissivity of polished copper, $\sigma = 5.67 \times 10^{-8}$ W/m^{2}K^4, and temperature is in units of Kelvin. Here the crystal operating temperature is specified to be ≈34 °C and a lab environment of 21 °C. The Peltier unit specifications were well in excess of these heating requirements with 2.25 W of heating or cooling capacity. This provided fast actuation between different selected temperatures and greater capacity for in air operation, typically more volatile due to convective disturbance due to air currents.

For the prototyping and testing stage of this experiment, frequent diagnostic measurements required the temperature offset well outside the phase matching window with offsets of 45 °C to operate the cavity without non-linear conversion. This was often done to check alignment and mode-matching with the homodyne detector in air and under vacuum. The fast actuation of the Peltier made switching operating modes of the OPO cavity convenient for prototyping and testing and had no apparent issues operating under vacuum.

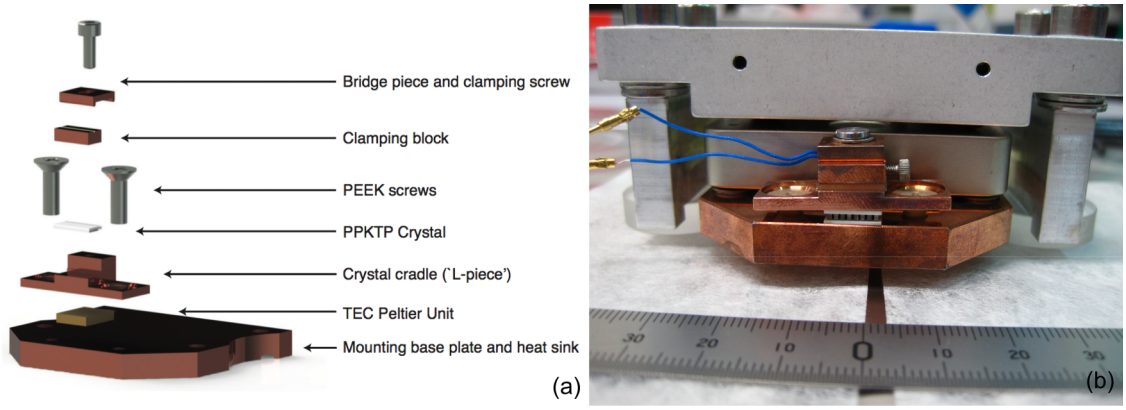

FIG. 5. (a) Exploded-view drawing of the oven assembly. Either side of the Peltier element and the PPKTP crystal is a thin sheet of indium foil (not shown) to improve thermal contact. (b) Photo of the assembled oven with mounting base plate and heat sink bolted to a four axis translation stage (Newport 8081M-UHV or similar). The translation stage itself is bolted upside-down to aluminium blocks that are glued to optical flats that are ready to be contacted to the glass breadboard. The structure is mounted on lens cleaning tissue for preliminary alignment to protect the surface of the glass breadboard.

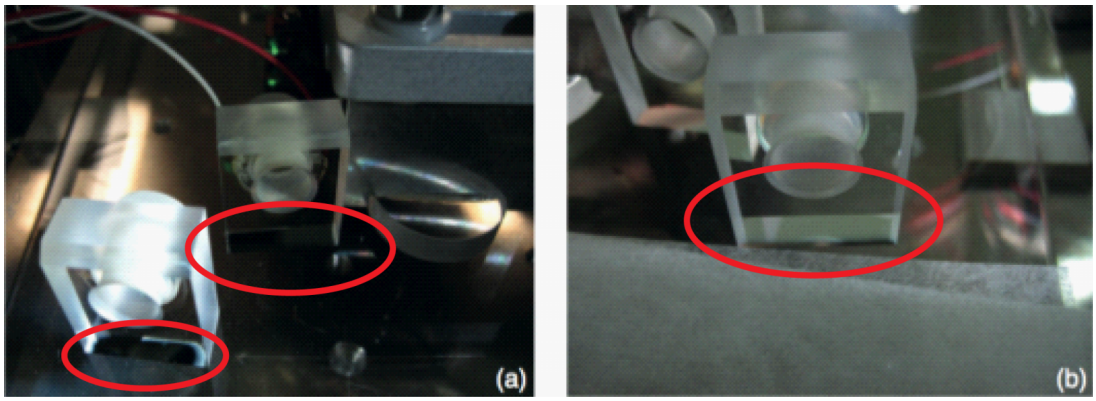

FIG. 6. Some examples of good and bad contacts are circled for clarity. (a) Suitable input coupler and curved mirror-prism contacts. Notice that on the left hand mirror that not all the area is contacted. This could be due to a dust particle or an artefact like a scratch. However there is a sufficient area bonded for confidence in the bond. Ultimately the RH curved mirror bond is more desirable. (b) Input coupler and curved mirror prism with a poor contact. There is a visible separation of surfaces (due to contamination and dust) such that it does not look optically continuous, as if it were a single material. The optic will lift off and the contact bonding process will need to be repeated.

III. OPTICAL RESONATOR CONSTRUCTION

The OPO cavity was assembled using two bonding techniques. The mirrors were bonded with epoxy to vertical fused silica mounting prisms (dimensions $25 \times 20 \times 10$ mm, Photon LaserOptik GmbH) as illustrated in Fig. 6. These assembled prisms were then attached to the $450 \times 150 \times 41$ mm polished fused silica breadboard (Sydor Optics) using solution-assisted optical contacting (Subsection III A). The entire assembly formed a rigid cavity into which the non-linear crystal was inserted. The thermally controlled crystal mount was in turn mounted on a four axis translation stage that was attached to the breadboard via optically contacted optical flats glued to aluminium post blocks. Together these elements formed a rigid non-linear cavity from which piezo electric transducer (PZT) voltage signals, temperature sensing, and actuation were routed to vacuum tank feedthrough.

The attachment of mirrors to the mounting prisms was achieved with small dots of degassed MasterBond EP30-2, a two part vacuum compatible epoxy. Gluing was required as the two curved mirrors were mounted on PZTs for cavity length control and the remaining mirrors had insufficient surface area about the holes to be confident of a good optical contact. Alignment rigs were used to centre mirrors (and curved mirror PZT's) on the prism holes with a small Viton o-ring used to elastically distribute pressure evenly about the mirrors while the epoxy was allowed to cure. The input-output coupler and HR flat mirror were glued directly to the prisms and the curved (ROC = −50 mm) mirrors were glued with matched Noliac PZTs (NAC2124-A01) sandwiched in between for cavity length actuation.

Finally the mirror-prism assemblies were optically contacted to the breadboard to form the bow-tie cavity of dimensions determined in Section II A. To guide and assist the alignment of the mirrors relative to each other, a precision alignment mask was manufactured on a CNC (Computer Numeric Control) machine with three contact points for each prism assembly.[29] Machining accuracy was accurate to ≈10 μm; however, micrometer adjustors were also included on the mask to provide a means to micro-align the yaw of the mirrors in establishing the intra-cavity mode. The mask assembly is pictured in Fig. 7.

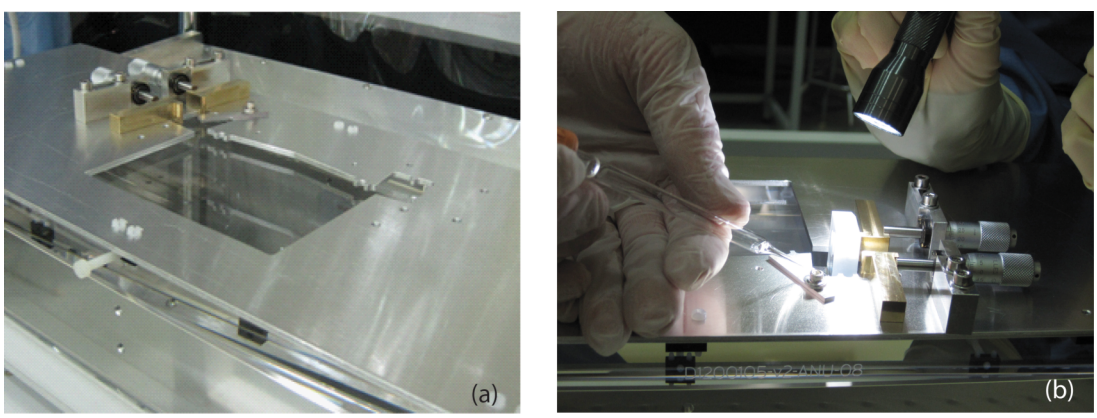

FIG. 7. (a) Cavity alignment mask mounted upon the glass breadboard with micrometers for fine angular alignment of the mirrors relative to each other. Extra space was cut out to allow the oven alignment rig to fit in. (b) A drop of methanol is applied while the mirror assembly continues to be aligned.

A. Optical contacting

Optical contacting is a direct intermolecular bond formed between two glass surfaces that are sufficiently smooth and clean such that their two surfaces seamlessly join when brought into direct mechanical contact.[30] There is no additional adhesive and the two surfaces are held together by Van der Waals forces and (when annealed) by covalent bonds. It has been found that for contact bonding, YRMS (RMS surface roughness) should ideally be less than 2 nm and preferably on the order 0.5 nm.[31] With the advent of modern polishing techniques, large flat surfaces can be fabricated, making possible the construction of extended flat glass breadboards to which glass components could be directly contacted, see, for example, Refs. 29, 32, and 33. The surface of the fused silica breadboard was specified to a flatness of $\lambda/10$ at a measurement wavelength of 632 nm. The surface has an RMS surface roughness of 6.3 ± 0.6 nm measured over a sub-aperture of 51 mm^2 (at the centre of the board) with a linear cross-sectional profile roughness of 5.1 ± 0.6 nm. This was above the ideal roughness mentioned above, but in practice was sufficient to form good optical contacts where the joints were clean from dust and other contaminants. Surfaces with more moderate surface flatness figures of $\lambda/4$ have been optically contacted.[29] The glass flats and prisms contacted to the glass breadboard had similar polishing specifications.

A dry optical contact immediately forms a bond. This makes aligning an OPO cavity with a tightly focused waist difficult to do accurately. In order to mediate the speed of the contact and to provide time to perform the micro-alignment process for each of the mirror-prism assemblies, a technique known as solution-assisted optical contacting was used.[33] After "drop-and-drag" tissue cleaning each of the two surfaces to be bonded, a small drop of spectroscopy grade methanol was placed between the contacting surfaces before they were brought together. The liquid layer moderates the distance and therefore the strength of the contact, providing a window of several minutes (depending on drop size) for adjusting the position before the surfaces "wring" together. Another desirable aspect of this bonding technique is that the period of adjustment may be extended indefinitely with additions of more solution. Complete reversal of the attempted bond may be accomplished by flooding the joint and applying a wiggling force to the mount. Care must be taken as the bond's uniform hold breaks rapidly and damage can be done to the board, the optic, or objects around. Usually the strength of the liquid capillary forces is such that removing the optic is easiest by sliding surfaces apart.

Figure 8 shows an example of a test optical contact between two $\lambda/10$ polished uncoated optical flats as the intermediary methanol evaporates and they "wring" together. The feel of the optics sliding past each other, mediated with the methanol layer, changes abruptly as they bond (it feels like a grinding stop). This bonding process is accompanied by the formation of etalon fringes. Counting the fringes and their spacing gives direct visual indication of the progress and quality of the bond as the last of the methanol is drawn out by capillary action between the surfaces. Bond failure will result in permanent fringes or an interface that is visibly not optically continuous. Cleanliness is paramount and contact bonding should be performed under conditions similar to those required for working with ultra-high vacuum environments.

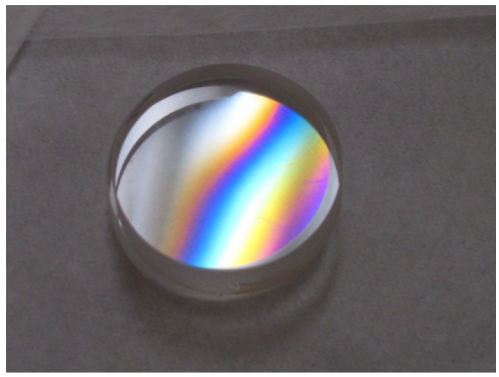

FIG. 8. Example of a contact bond in progress. The fringes were formed as the alcohol layer dissipated and the contact bond begins to take hold, known as "wringing" together. A poor contaminated join stops at this point. Only when full fringes vanish across the polished portions of the surface, indicating a seamless joint with no etalon gap, is the bond completed.

B. Positioning optical resonator optics

The alignment mask was rested on its PEEK support lugs and where appropriate all tools and parts were cleaned in a ultrasonic bath (with Liquinox) then rinsed, wiped, and finally wiped down with methanol. All parts associated with the oven build (Section II C) were handled wearing modest cleanroom apparel suitable for a class 10 000 cleanroom.

The following procedure was used for the alignment of mirrors to form a bow-tie cavity mode:

1. Clean breadboard and tombstones immediately before the mask placement.
2. A 532 nm (visible) beam was mode matched to the expected waist position in the cavity to be built with waist of $(141_s, 133_t)$ μm.
3. Before a build using optical contacting, it was useful to place optics on the board with thin lens tissue between the mirror mounts and the board, to protect the polished surfaces. In this way, it was possible to build a practice cavity, so that the mask could be positioned relative to the input beam, and the micrometer positions for optic placement could be finalised.
4. The mask was set down with the fixing screws and the beam was aligned to pass square through the centre point of the designated mirror positions. Swabbing with optics tissue to clear any newly settled dust, a single drop of methanol was applied to the breadboard and the HR flat mirror was placed on the board. While it was still sliding freely, it was moved into position, resting on the three contact points machined into the mask. The input beam was adjusted so that the beam was centred on the mirror and adjusted so that the angle subtended by the outgoing beam was 12° and parallel to the board. Manual pressure

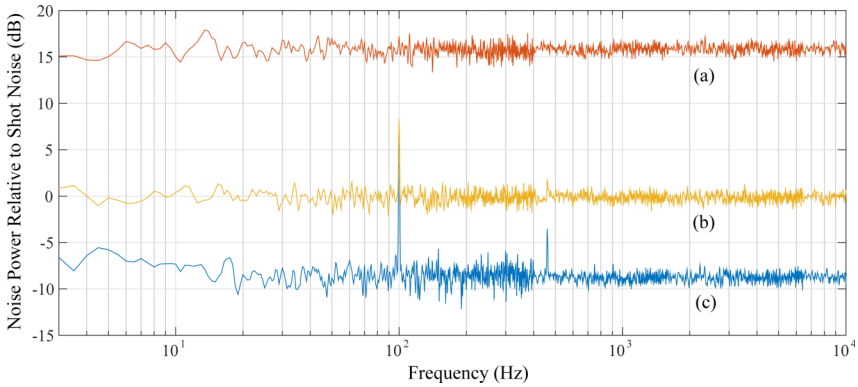

FIG. 9. Noise power relative to shot noise. (a) Anti-squeezing (15.9 ± 0.7 dB), (b) shot noise, and (c) squeezing (8.6 ± 0.9 dB). Spikes are cross talk from electronic noise. The data were stitched together from 5 separate spans; 102.4 kHz, 25.6 kHz, 6.4 kHz, 1.6 kHz, 400 Hz. The first 4 spans have 100 averages, and the last has 50. Adapted from Ref. 13.

was placed on the optic while the bond was left to dry and set.

5. The first curved mirror was then placed in a similar manner and adjusted so that the reflected beam was parallel with the input beam. Curved mirror alignment is typically more sensitive to angular perturbations from ideal, so optimisation is best focused on the curved mirror alignment.
6. The second curved mirror was positioned such that the AOI was 6° and overlapped with the input beam at the input coupler position.
7. The input coupler was positioned and finely adjusted, until multiple round trips of the cavity were visible. Note that while without the crystal, the cavity is unstable, multiple round trips were visible and a sufficient guide for a rough first alignment.
8. With the cavity mirrors set, the oven legs were contacted such that the oven was centered with respect to the two curved mirrors. The oven translation stage was adjusted so that the cavity mode cleared the crystal aperture. Care must be taken not to wet joints of already bonded components.

IV. OPO SQUEEZING PERFORMANCE

The OPO was pumped with 105 mW of second harmonic (532 nm) light and locked to the cavity resonance with a Pound-Drever-Hall (PDH) control scheme that actuated on the OPO PZT's. The shift in the dispersion when moving from air to vacuum was carefully calculated and a nonlinear gain of 16 was measured. The phase of the squeezing ellipse was controlled with the technique of modified coherent sideband locking[11,22] and the balanced homodyne detection system was designed to mitigate scattering as much as possible and had 70 dB of common mode rejection for the local oscillator noise.[34]

This system was able to deliver 8.6 dB of squeezed light in the audio band to frequencies as low as 10 Hz[13] (Fig. 9) and has remained operational in vacuum at this level of performance for several months. The semi-monolithic glass OPO performs well and can be reliably reconstructed where the greatest difficulty is to ensure that the glass surfaces are sufficiently clean, smooth, and flat. The biggest limitation of the current system is due to a number of auxiliary control systems that limit the length of time squeezed light can be measured to periods of around an hour. A full system analysis of all the control loops and subsequent automation will be required to ensure the continuous production of squeezed light necessary for use in a GW detector. For full experimental details of the generation of squeezed light using the OPO described in this article see Ref. 13.

ACKNOWLEDGMENTS

We acknowledge discussions with the Quantum Measurement group at MIT, the Advanced LIGO Output Mode Cleaner team, the LIGO Scientific Collaboration, and Professor Roman Schnabel and Dr. Henning Vahlbruch of the AEI. This research was supported by the Australian Research Council under the Discovery Program No. DP14010098.

[1]J. Abadie *et al.*, Nat. Phys. **7**, 962–965 (2011).
[2]S. S. Y. Chua, B. J. J. Slagmolen, D. A. Shaddock, and D. E. McClelland, Classical Quantum Gravity **31**, 183001 (2014).
[3]R. Schnabel, N. Mavalvala, D. E. McClelland, and P. K. Lam, Nat. Commun. **1**, 121 (2010).
[4]E. Oelker, L. Barsotti, S. Dwyer, D. Sigg, and N. Mavalvala, Opt. Express **22**, 21106–21121 (2014).
[5]H. Grote *et al.*, Phys. Rev. Lett. **110**, 181101 (2013).
[6]J. Aasi *et al.*, Nat. Photonics **7**, 613–619 (2013).
[7]K. L. Dooley, J. R. Leong, T. Adams, C. Affeldt, A. Bisht, C. Bogan, J. Degallaix, C. Gräf, S. Hild, J. Hough, A. Khalaidovski, N. Lastzka, J. Lough, H. Lück, D. Macleod, L. Nuttall, M. Prijatelj, R. Schnabel, E. Schreiber, J. Slutsky, B. Sorazu, K. A. Strain, H. Vahlbruch, M. Was, B. Willke, H. Wittel, K. Danzmann, and H. Grote, LIGO Technical Document, LIGO-P1500140–v3, 2015.
[8]A. Ciapponi, W. Riede, G. Tzeremes, H. Schröder, and P. Mahnke, Proc. SPIE **7912**, 791205 (2011).
[9]Z. Tang *et al.*, Sci. Rep. **4**, 6366 (2014).
[10]D. H. Chang, I. Y. Poberezhskiy, and J. L. Mulder, Proc. SPIE **6713**, 67130U-1–67130U-13 (2007).
[11]S. S. Y. Chua, M. S. Stefszky, C. M. Mow-Lowry, B. C. Buchler, S. Dwyer, D. A. Shaddock, P. K. Lam, and D. E. McClelland, Opt. Lett. **36**, 23 (2011).
[12]M. S. Stefszky, Ph.D. thesis, The Australian National University, 2012.
[13]A. R. Wade, G. L. Mansell, S. S. Y. Chua, R. L. Ward, B. J. J. Slagmolen, D. A. Shaddock, and D. E. McClelland, Sci. Rep. **5**, 18052 (2015).
[14]H. Vahlbruch *et al.*, Classical Quantum Gravity **27**, 084027 (2010).
[15]A. Khalaidovski *et al.*, Classical Quantum Gravity **29**, 075001 (2012).

[16]E. Oelker, L. Barsotti, S. Dwyer, D. Sigg, and N. Mavalvala, Opt. Express **22**, 21106 (2014).
[17]S. Dwyer, L. Barsotti, S. S. Y. Chua, M. Evans, M. Factourovich, D. Gustafson, T. Isogai, K. Kawabe, A. Khalaidovski, P. K. Lam, M. Landry, N. Mavalvala, D. E. McClelland, G. D. Meadors, C. M. Mow-Lowry, R. Schnabel, R. M. S. Schofield, N. Smith-Lefebvre, M. Stefszky, C. Vorvick, and D. Sigg, Opt. Express **21**, 19047–19060 (2013).
[18]K. Arai, S. Barnum, P. Fritschel, J. Lewis, and S. Waldman, LIGO Technical Note, LIGO-T1000276–v5, 2013.
[19]J.-Y. Vinet, V. Brisson, S. Braccini, I. Ferrante, L. Pinard, F. Bondu, and E. Tournie, Phys. Rev. D **56**, 6085–6095 (1997).
[20]J.-Y. Vinet, V. Brisson, and S. Braccini, Phys. Rev. D **54**, 1276–1286 (1996).
[21]D. J. Ottaway, P. Fritschel, and S. J. Waldman, Opt. Express **20**, 8329 (2012).
[22]H. Vahlbruch, S. Chelkowski, B. Hage, A. Franzen, K. Danzmann, and R. Schnabel, Phys. Rev. Lett. **97**, 043814 (2006).
[23]G. D. Boyd and D. A. Kleinman, J. Appl. Phys. **39**, 3597–3639 (1968).
[24]A. E. Siegman, *Lasers* (University Science Books, 1986).
[25]T. McRae, A. Wade, R. Ward, and B. Slagmolen, LIGO Technical Note, LIGO-T1500350–v1, 2015.
[26]K. Goda, Ph.D. thesis, Massachusetts Institute of Technology, 2007.
[27]S. S. Y. Chua, Ph.D. thesis, The Australian National University, 2013.
[28]M. Stefszky, C. M. Mow-Lowry, K. McKenzie, S. Chua, B. C. Buchler, T. Symul, D. E. McClelland, and P. K. Lam, J. Phys. B: At., Mol. Opt. Phys **44**, 015502 (2011).
[29]G. DeVine, B. Ware, D. M. Wuchenich, R. E. Spero, W. M. Klipstein, and K. McKenzie, NASA Tech. Briefs, May 2012, p. 36 (SEE 20120009218).
[30]J. Haisma and G. A. C. M. Spierings, Mater. Sci. Eng., R **37**(1-2), 1–60 (2002).
[31]T. Abe, M. Nakano, and T. Itoh, in *Silicon-on-Insulator Technology and Devices*, edited by D. N. Schmidt (Electrochemical Society, Pennington, USA, 1990), p. 61.
[32]C. Braxmaier, G. Heinzel, K. F. Middleton, M. E. Caldwell, W. Konrad, H. Stockburger, S. Lucarelli, M. B. te Plate, V. Wand, A. C. Garcia, F. Draaisma, J. Pijnenburg, D. I. Robertson, C. Killow, H. Ward, K. Danzmann, and U. A. Johann, Proc. SPIE **5500**, 164 (2004).
[33]D. A. Shaddock and A. Abramovici, NASA Tech. Briefs, March 2004, p. 27 (SEE 20110016643).
[34]M. S. Stefszky, C. M. Mow-Lowry, S. S. Y. Chua, D. A. Shaddock, B. C. Buchler, H. Vahlbruch, A. Khalaidovski, R. Schnabel, P. K. Lam, and D. E. McClelland, Classical Quantum Gravity **29**, 14 (2012).